HHS Public Access

Author manuscript

Dev Cell. Author manuscript; available in PMC 2017 December 19.

Published in final edited form as:

Dev Cell. 2016 December 19; 39(6): 653–666. doi:10.1016/j.devcel.2016.11.008.

Regionally Restricted *Hox* Function in Adult Bone Marrow-Multipotent Mesenchymal Stem/Stromal Cells

Danielle R. Rux[1], **Jane Y. Song**[2], **Ilea T. Swinehart**[3,**], **Kyriel M. Pineault**[1], **Aleesa J. Schlientz**[3,***], **Kelsey G. Trulik**[3], **Steve A. Goldstein**[4], **Ken M. Kozloff**[4], **Daniel Lucas**[1], and **Deneen M. Wellik**[1,2,3,5,*]

[1]Department of Cell and Developmental Biology, University of Michigan, Ann Arbor, MI 48109-2200, USA

[2]Cellular and Molecular Biology Program, University of Michigan, Ann Arbor, MI 48109-2200, USA

[3]Department of Internal Medicine, Division of Molecular Medicine and Genetics, University of Michigan, Ann Arbor, MI 48109-2200, USA

[4]Department of Orthopedic Surgery, University of Michigan, Ann Arbor, MI 48109-2200, USA

Summary

Posterior *Hox* genes (*Hox9-13*) are critical for patterning the limb skeleton along the proximodistal axis during embryonic development. Here we show that *Hox11* paralogous genes, which developmentally pattern the zeugopod (radius/ulna and tibia/fibula), remain regionally expressed in the adult skeleton. Using *Hoxa11eGFP* reporter mice, we demonstrate expression exclusively in multi-potent mesenchymal stromal cells (MSCs) in the bone marrow of the adult zeugopod. Hox-positive cells express PDGFRα and CD51, are marked by *LepR-Cre*, exhibit CFU-F activity and tri-lineage differentiate *in vitro*. Loss of *Hox11* function leads to fracture repair defects, including reduced cartilage formation and delayed ossification. *Hox* mutant cells are defective in osteoblastic and chondrogenic differentiation in tri-lineage differentiation experiments and these defects are zeugopod-specific. In the stylopod (humerus and femur) and sternum, BM-MSCs express other regionally restricted *Hox* genes and femur fractures heal normally in *Hox11* mutants. Together, our data supports regional *Hox* expression and function in skeletal MSCs.

[*]Corresponding Author: Deneen M. Wellik, PhD, dwellik@umich.edu, University of Michigan Medical Center, 109 Zina Pitcher, 2053 BSRB, Ann Arbor, MI 48109-2200, Phone: 734-936-8902, FAX: 734-763-2162.
[5]Lead Contact
[**]Current address: MedPace Incorporated, Cincinnati, OH 45227
[***]Current address: Institute of Molecular Biology, University of Oregon, Eugene, OR 97403

Supplemental Information

Supplemental Information for this article includes seven figures.

Author Contributions

Conceptualization: D.M.W., D.R.R. and D.L., Methodology: S.A.G. and K.M.K. Investigation: D.R.R., J.Y.S., K.M.P., I.T.S., A.J.S., D.L., S.A.G., K.M.K., K.G.T. Validation: S.A.G. and K.M.K. (new fracture methodologies). Writing – Original Draft: D.R.R. and D.M.W., Writing – Review & Editing: D.M.W., D.R.R., D.L.; Funding Acquisition: D.M.W., D.R.R., K.M.P. and J.Y.S. Supervision: D.M.W.

Graphical Abstract

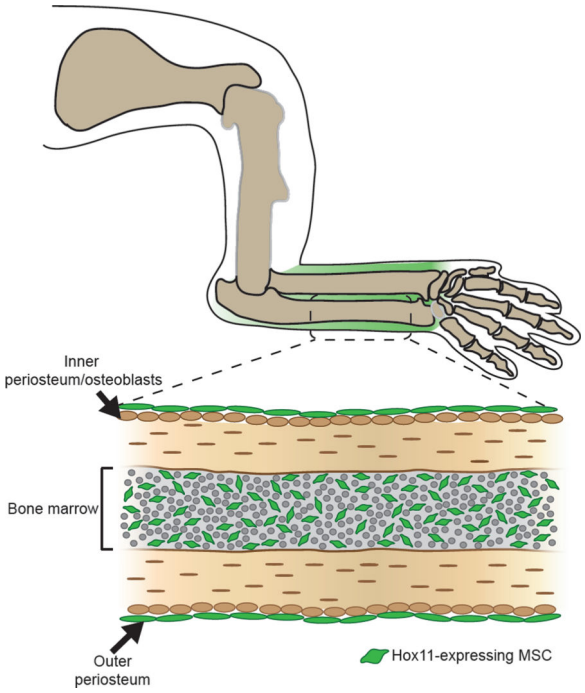

Introduction

Hox genes are responsible for critical patterning events along regionally restricted, overlapping domains of the anteroposterior axis of the axial skeleton (Mallo et al., 2010). In addition to this highly conserved role, the posterior *Hox* group genes 9 through 13 play critical roles in the development of the proximodistal skeleton of the limbs (Davis et al., 1995; Fromental-Ramain et al., 1996a; Fromental-Ramain et al., 1996b; Wellik and Capecchi, 2003). *Hox9* and *Hox10* function is required for patterning the most proximal element of the limb, the stylopod (femur and humerus) (Fromental-Ramain et al., 1996a; Raines et al., 2015; Wellik and Capecchi, 2003). *Hox11* genes are required for the middle limb elements or zeugopod (radius and ulna; tibia and fibula) (Davis et al., 1995; Wellik and Capecchi, 2003), and the *Hox13* group genes are critical for establishment of the autopod skeleton (carpals and metacarpals; tarsals and metatarsals) (Fromental-Ramain et al., 1996b).

The establishment of the spatial restriction of *Hox* expression has been investigated in detail (Lonfat and Duboule, 2015; Montavon and Duboule, 2013), but much less is understood regarding how *Hox* genes function in establishing skeletal morphologies and pattern that are unique to each region of the vertebrate skeleton. In an attempt to gain insight into this question, we previously generated and examined a GFP insertion allele in one of the *Hox11* paralogs, *Hoxa11* (Nelson et al., 2008). In the developing limb, expression initiates broadly in the limb bud mesenchyme. As Sox9-expressing cells condense to form the two zeugopod anlage (radius/ulna or tibia/fibula), Hoxa11eGFP expression is excluded from these cells and becomes localized to the outer perichondrium surrounding these elements as they condense

and grow (Nelson et al., 2008; Swinehart et al., 2013). *Hoxd11* is expressed with a similar pattern, suggesting that the paralogs are expressed in the same cells (Pineault et al., 2015). As the cartilage matures and bone formation initiates, *Hox* expression remains excluded from differentiated cell types. Hoxa11eGFP is not expressed in differentiating cartilage, in osteoblasts, or in endothelial cells in the limb. During developmental stages, Hoxa11eGFP is only expressed in the outer perichondrial stromal cells just outside the osteoblast layer surrounding both zeugopod elements and it persists through newborn stages (Nelson et al., 2008; Swinehart et al., 2013).

In this study, we pursue analyses of these Hoxa11eGFP-positive cells into postnatal and adult stages. We find that the pattern of *Hox11* expression established during development is maintained through postnatal and adult stages in the periosteum of the adult animal. Intriguingly, we find that Hoxa11eGFP becomes additionally visualized in the bone marrow. We identify these adult Hoxa11eGFP-positive cells as a population of bone marrow – multi-potent mesenchymal stem/stromal cells (BM-MSCs) (Kfoury and Scadden, 2015). *In vivo*, Hoxa11eGFP-expressing cells are identified by three cell surface markers: PDGFRα, CD51, and Leptin Receptor, and they expand at the site of injury following fracture. *In vitro, Hox11*-expressing cells are capable of tri-lineage differentiation (to osteoblasts, chondrocytes and adipocytes) and they exhibit greater self-renewal potential (colony forming unit-fibroblast, CFU-F) than previously described MSC populations. In addition, we find that *Hox11* functions in these cells *in vitro* for proper differentiation to the mesenchymal osteogenic and chondrogenic lineages and that lineage-labeled Hoxa11eGFP-positive cells transplanted into a fracture callus can differentiate to both cartilage and bone. Importantly, we show that *Hox11* genes maintain region specific expression upon fracture injury and that this regional *Hox*-positive population is functionally important in fracture repair. *Hox11* mutant animals have significant defects in repair of the zeugopod, with decreased cartilage formation and delayed osteogenesis *in vivo*. Taken together, our data shows that *Hox* genes are exclusively expressed in region-specific adult BM-MSCs and that *Hox* function is critical for regional osteochondral progenitor activity of MSCs *in vitro* and *in vivo*.

Results

Hox11 expression is maintained in undifferentiated stromal cells through postnatal and adult stages

We have previously shown that Hoxa11eGFP becomes localized to the zeugopod (radius/ulna or tibia/fibula) region during embryonic stages and is observed in the perichondrium surrounding the skeletal elements where it persists through newborn stages (Figure S1 and Nelson et al. 2008; Swinehart et al. 2013). Maintenance of this expression through developmental stages prompted us to examine expression at postnatal and adult stages using this knock-in reporter. We find that Hoxa11eGFP remains restricted to the zeugopod region of both forelimbs and hindlimbs, consistent with the regional expression observed during development (Figure 1A, S1A and S2A). Further, we find that the perichondrial expression established in the embryo is preserved in the periosteal region through adult stages (Figure 1B, S1B, S2B and S2C). Additionally, during postnatal growth, Hoxa11eGFP expression

becomes visualized at the endosteal surface of the zeugopod bone and throughout the bone marrow (Figure 1B, S2B and S2C). *Hoxd11* exhibits a similar expression pattern, consistent with both *Hox11* paralogs functioning in the postnatal and adult skeleton (Pineault et al., 2015). Consistent with what we have previously shown at embryonic stages, Hoxa11eGFP expression does not overlap with any differentiated cell types in the adult skeleton; expression is excluded from macrophages, endothelial cells, adipocytes, neurons, osteoblasts and osteoclasts (Figure 2A–G) (Swinehart et al., 2013). Of note, high magnification visualization of Hoxa11eGFP reveals a distinct stromal appearance, and many GFP-positive cells are observed in close association with bone marrow vasculature (Figure 2B). Taken together, these observations led us to explore whether Hoxa11eGFP-expressing cells are a mesenchymal progenitor population.

Adult *Hox11*-expressing cells are MSCs

Bone marrow is comprised largely of hematopoietic cells (~98–99%), while the remaining 1–2% of cells are bone marrow stromal cells. Among stromal cells, approximately 15% are endothelial cells with the remaining 85% termed non-endothelial stroma. Bone marrow multipotent mesenchymal stem/stromal cells (BM-MSCs) are contained within the non-endothelial stromal population, but comprise only a small subset (~5%) of these cells (Kfoury and Scadden, 2015). In recent years, a number of methods have been described that enrich for BM-MSCs with high progenitor activity. Co-labeling with cell surface markers PDGFRα and CD51, and genetic lineage labeling using *Leptin Receptor-Cre* (*LepR-Cre*) are two methods that have been reported to most highly enrich for mesenchymal progenitor cell activity (Kunisaki et al., 2013; Pinho et al., 2013; Zhou et al., 2014).

Using FACS analyses, we examined the bone marrow from zeugopods of *Hoxa11eGFP* heterozygous mice, and we find that GFP-positive cells are not observed in the hematopoietic compartment (CD45+Ter119+) and do not sort with the endothelial stroma (CD31+, Figure 3A and S3A). Hoxa11eGFP-positive cells sort entirely within the non-endothelial stromal compartment with the majority of GFP-positive cells additionally marked by both PDGFRα and CD51 (Figure 3B, and S3A–B). We additionally find that Hoxa11eGFP-expressing cells are Leptin Receptor (LepR)-positive using an antibody to LepR for FACS analyses (Figure 3C and S3A). To examine this further, we generated mice carrying a single allele of *Hoxa11eGFP*, *LepR-Cre*, and *ROSA-LSL-tdTomato* (DeFalco et al., 2001; Madisen et al., 2010; Nelson et al., 2008). Bone marrow was examined at adult stages, and virtually all Hoxa11eGFP-expressing cells in these populations were co-labeled with ROSA-Tomato (LepRiTom, Figure 3D and S4A). These data suggest that Hoxa11eGFP-postive cells represent a subset of BM-MSCs within this previously defined population. Interestingly, we find that Hoxa11eGFP-positive periosteal cells lining the surface of the zeugopod skeletal elements also demonstrate high co-expression with PDGFRα/CD51 and, to a lesser extent, LepR (Figure 3E–F, and S3C). Of note, Hoxa11GFP-positive cells were not detected in any populations of non-GFP animals or in the stylopod (humerus) of *Hoxa11eGFP*+/− animals, consistent with maintenance of the regionally restricted *Hox* expression pattern that is established during development (Figure S4B).

Hallmark functions of BM-MSCs include self-renewal and differentiation into mesenchymal lineages. If Hoxa11eGFP-expressing cells are mesenchymal progenitor cells, sorted Hoxa11eGFP-positive cells should be capable of tri-lineage differentiation into chondrocytes, osteoblasts and adipocytes and should be able produce self-renewing fibroblast colony-forming units (CFU-Fs) *in vitro*. These assays were performed and we find that Hoxa11eGFP-positive cells are able to differentiate into all three lineages (Figure 3G). Interestingly, examination of CFU-F formation reveals very high progenitor activity in the Hoxa11eGFP-positive BM-MSCs. Figure 3H shows that PDGFRα /CD51 double-positive cells show significant CFU-F potential as previously published (Pinho et al., 2013). When zeugopod bone marrow cells are additionally sorted for Hoxa11eGFP (PDGFRα /CD51/ Hoxa11eGFP triple-positive), these cells demonstrate approximately three-fold higher CFU-F activity than cells sorted only for PDGFRα and CD51 (Figure 3H). Combined, these data strongly support that Hoxa11eGFP-positive bone marrow stromal cells represent a mesenchymal stem/progenitor population.

Hox11 functions during fracture repair and maintains regional specificity

It has been previously demonstrated that MSCs expand in response to fracture injury and are required for repair (Gerstenfeld et al., 2003; Mizoguchi et al., 2014; Park et al., 2012; Schindeler et al., 2008; Shapiro, 2008; Worthley et al., 2015; Zhou et al., 2014). To examine whether Hoxa11eGFP-positive cells display this response, we fractured the zeugopod of *Hoxa11eGFP* heterozygous animals (forelimb ulna or hindlimb tibia, in separate analyses) and show that Hoxa11eGFP-positive cells expand at the site following injury (Figure 4A). *Hox11*-expressing cells do not overlap with differentiated cell types, including macrophages, endothelium, osteoblasts or osteoclasts, during repair (Figure 4B–E). We observe Hoxa11eGFP-expressing cells are highly associated with the vasculature in the fracture callus and that, during soft callus formation, the highest expression of Hoxa11eGFP is in cells surrounding the callus, largely excluded from the Sox9-expressing differentiating chondrocytes closer to the center of the callus (although we note a small number of cells with overlapping expression in areas that appear to be transitioning from stromal cells to chondrocytes as we previously reported at embryonic stages, Figure 4E and F, (Swinehart et al., 2013)).

We find that the expanded Hoxa11eGFP-positive population sorts with the same FACS profile observed prior to fracture – non-hematopoietic, non-endothelial stromal cells that are double-positive for both PDGFRα and CD51, as well as co-labeled *in vivo* using LepR-Cre (Figure 5A and B). Interestingly, we find that this PDGFRα+/CD51+ profile is maintained throughout the fracture repair process (Figure 5C and S5A–B). Together, these observations are consistent with the cellular activity expected for MSCs following fracture injury.

To further test the potential of these cells in fracture repair, LepRiTom+/Hoxa11eGFP+ cells from adult bone marrow were transplanted into the four-day old fracture callus of wild-type animals. While transplanted MSCs are not capable of integrating to re-populate the bone marrow niche, previously published work shows that a small fraction of progenitor-enriched MSCs injected into a fracture callus are capable of differentiating into cartilage and bone under these transplant conditions (Park et al., 2012; Worthley et al., 2015; Zhou et al., 2014).

Figure 5D shows the fracture callus six days after transplantation (10 days post-fracture). Hoxa11eGFP-positive cells lineage-labeled by *LepR-Cre;ROSA-LSL-tdTomato* and injected into the fracture callus of a wild-type animal are capable of differentiating to Sox9-positive chondrocytes and Osterix-positive osteoblasts after transplantation (Figure 5D).

Data presented herein strongly supports the assertion that Hoxa11eGFP marks an MSC population. Further, MSCs are the only cell population in which Hoxa11eGFP-positive cells can be identified; Hoxa11eGFP expression is not observed in any differentiated cell types of the skeleton. To provide evidence regarding whether *Hox* genes function in the context of the adult skeleton *in vivo*, we performed fracture analyses on *Hox11* compound mutants (animals in which three of the four functioning *Hox11* alleles are mutated, *11Aadd*) and littermate controls (*Hoxa11eGFP* heterozygous, $11Aa^{G}$, mice and wild-type, *11AADD*, mice, which were indistinguishable in these experiments). Control mice heal normally, ossifying across the fracture gap by 3 weeks post-fracture (WPF) and remodeling almost completely by 12 WPF (Figure 6A). In fractures of *Hox11* compound mutant mice, ossification across the fracture gap is delayed, although most show a completely ossified callus by 6 WPF. Even by 12 WPF, *Hox11* compound mutants do not approach the level of repair observed in controls (Figure 6A). These observations were quantified using a rated scale and blind scoring of microCT images in two orthogonal visual planes (Figure 6B).

Unstabilized fractures, like the ulnar fractures described here, typically heal through endochondral ossification whereby new bone is formed from a cartilage anlagen (Gerstenfeld et al., 2003; Schindeler et al., 2008). We find that cartilage formation is reduced in the compound mutants and the amount of cartilage produced never reaches the levels observed in controls (Figure 6C). Importantly, Hoxa11eGFP-positive cells in compound mutant animals display the same FACS profile observed in control animals. The proportion of Hoxa11eGFP-positive cells in the bone marrow of controls and of compound mutants is also unchanged (Figure 6D–E, and S6A–B). Additionally, the CFU-F capacity of Hoxa11eGFP-positive cells from compound mutant animals is not diminished compared to controls (Figure 6F). Together, these results demonstrate that the defects in skeletal healing are not due to a diminished number of MSCs, but that the *Hox11* mutant MSCs are not capable of the proper differentiation required to produce the cell types required for efficient repair.

If the defects in skeletal healing result from loss of *Hox11* function in the MSC population, *Hox11* mutant MSCs should show similar defects during *in vitro* differentiation assays. To assess this, we performed tri-lineage differentiation on Hoxa11eGFP-positive cells from control and *Hox11* mutant animals. In these assays, isolated mutant Hoxa11eGFP-positive cells are defective in osteogenic and chondrogenic differentiation *in vitro*, analogous to what is observed *in vivo*. Intriguingly, *Hox11* mutant cells in this assay exhibit an increased propensity to differentiate to adipose cells compared to controls (Figure 6G). Combined with *in vivo* fracture data, these analyses strongly support *Hox11* gene function in adult MSCs in regulating skeletal cell differentiation.

An important characteristic of *Hox* expression, developmentally, is the restriction of paralog expression along the anteroposterior axis of the axial skeleton and the proximodistal axis of

the limbs. Here, we demonstrate that adult limbs maintain the same zeugopod-specific expression of Hoxa11eGFP that is observed developmentally. If *Hox*-expressing MSCs serve as a regionally restricted mesenchymal progenitor population, we should not observe expression of Hoxa11eGFP in other skeletal areas and there should be no defects in fracture repair in *Hox11* compound mutants in other regions of the skeleton where they are not normally expressed. This is supported by experiments in which the stylopod (femur) of *Hox11* compound mutants and controls were fractured and followed after injury to assess healing. Figure 7A (and Figure S7) shows that Hoxa11eGFP expression is not initiated ectopically upon injury in this region (Figure 7A and S7). Further, there are no differences between controls and *Hox11* compound mutant animals in repair of the femur in response to fracture injury (Figure 7B). Thus, *Hox11* functions in a regionally restricted manner in this process.

Further support for regional *Hox* expression and function is supported by qPCR analyses of bone marrow stromal cells from other regions of the skeleton. In these experiments, stromal cells from the stylopod and zeugopod were isolated and expanded separately. Stylopod stromal cells exhibit preferential expression of *Hox9* and *Hox10* genes, with low *Hox11* gene expression. In zeugopod stromal cells, *Hox11* genes are preferentially expressed over the adjacent *Hox* genes (Figure 7C), mirroring the *Hox* expression profile observed *in vivo*. We additionally sorted and performed qRT-PCR on LepRiTom-positive and LepRiTom-negative non-endothelial stromal cells (CD45-TER119-CD31-) from fresh bone marrow from the stylopod, zeugopod, and sternum. Due to limited cell number, we analyzed only a small set of *Hox* genes, but we find that these cells also display a *Hox* expression profile that is consistent with regional, embryonic expression patterns. *Hoxa9* and *Hoxa10* are expressed in the stylopod, but not the zeugopod. *Hoxa11* is expressed in the zeugopod, but not the stylopod or the sternum, and *Hoxa5*, *Hoxb6*, and *Hoxc6* are expressed in the sternum (Figure 7D). These analyses further show *Hox* expression is observed exclusively in the Leptin Receptor lineage labeled cells. *Hox* expression is not detected in any Leptin Receptor-negative, non-endothelial stromal cells from any region examined.

Discussion

Taken together, numerous lines of evidence support Hoxa11eGFP-positive zeugopod cells as a regional, functionally relevant BM-MSC population in adult animals. Hoxa11eGFP-positive cells are a non-endothelial stromal population that express cell surface markers that define MSCs (PDGFRα, CD51 and LepR), are lineage-traced with *LepR-Cre*, demonstrate high CFU-F activity and tri-lineage differentiate *in* vitro, and expand in response to fracture. Further, Hoxa11eGFP expression in the adult bone is found exclusively in the non-endothelial stromal PDGFRα-positive, CD51-positive and LepR-positive MSC population in the skeleton with no expression observed in any differentiated cells of the skeleton. This builds on work reported by others that have previously shown that regionally-restricted *Hox* expression persists in adult fibroblast populations (Ackema and Charite, 2008; Chang et al., 2002; Leucht et al., 2008; Rinn et al., 2006; Rinn et al., 2008). The current work represents the first demonstration that Hox-positive cells can be identified as regionally restricted BM-MSCs and function in this population of cells in the differentiation of skeletal lineages *in vivo*. *Hox11* mutants are unable to repair properly in response to zeugopod injury, exhibiting

reduced cartilage formation and delayed osteogenic bridging, but show no defects in repair of the stylopod. *In vitro*, *Hox11* mutant MSCs are unable to differentiate into skeletal lineages. The collective phenotypes through development, postnatal growth and adult stages are consistent with a model whereby *Hox* genes regulate the proper differentiation of MSCs to mesenchymal skeletal lineages throughout the life of the animal.

The data reported herein demonstrates continuous Hoxa11eGFP expression through postnatal and adult stages in the periosteum of the zeugopod skeleton, with increased and persistent expression in bone marrow stromal cells exclusively in progenitor-enriched BM-MSCs. Our previously published work examining expression through embryonic stages showed that expression is restricted to the zeugopod perichondrium during early stages of limb development and that this perichondrial/periosteal expression is maintained through newborn stages (Nelson et al., 2008; Swinehart et al., 2013). It is interesting to correlate real-time Hoxa11eGFP reporter expression with results from a recent study that closely examined the lineage-tracing profile of a conditionally activated *Osterix-Cre (Osx-Cre^{ERT2})*. When *Osx-Cre^{ERT2}* activity is induced at early postnatal stages, a subset of lineage-traced cells that are initially labeled perichondrium/periosteum become long-lived BM-MSCs that can be observed in the adult bone marrow (Mizoguchi et al., 2014). In future studies, it will be important to compare the lineage-labeled populations marked by this and other Cre lines with the Hoxa11eGFP reporter to understand the relationships between *Hox11*-expressing MSCs and these lineages. Additionally, it will be important to examine the lineage contribution of *Hox*-expressing cells from development through embryonic, postnatal and adult stages. Our results are consistent with the possibility that the *Hox*-expressing cells that become regionally restricted during embryogenesis give rise to postnatal progenitors and long-term adult MSC population, but this possibility will require further testing in future experiments.

Whether other *Hox* paralogous group genes function in MSCs in other skeletal regions will be a very interesting question to pursue in future studies. The preservation of the regionally restricted, differential *Hox* expression that is established during development exclusively in progenitor-enriched MSCs from the adult stylopod and sternum in addition to the zeugopod supports this possibility. Perhaps the most intriguing new question raised by this work is whether distinct *Hox* paralogs impart differential functional information within these regional MSC populations that inform patterning, repair, and morphology of specific regions of the skeleton. This has been clearly shown to be the case genetically during development, but will be critical to compare and examine at adult stages in MSCs.

Regionalized expression of *Hox* genes in MSC populations adds a new level of complexity to the increasingly broad roles that skeletal MSCs perform in the adult animal. Our data indicate that skeletal progenitor cells have regional signatures of *Hox* gene expression that are functionally relevant, at least for the *Hox11* paralogous group. If regional BM-MSC populations possess unique functional characteristics imparted by differential *Hox* expression, there are critical implications for use of mesenchymal progenitor cells obtained from bone marrow in regenerative therapies (Bianco et al., 2013; Frenette et al., 2013). It is possible that the location from which MSCs are isolated and the *Hox* profile they express have important influences on how they behave *in vivo, in vitro*, and in transplantation for

regenerative purposes. This should be further explored and considered in therapeutic approaches using MSCs.

Experimental Procedures

Mice

All mice were maintained in a C57BL/6 background. Male and female mice either double or single heterozygous for the *Hoxa11* and *Hoxd11* null alleles were mated to generate compound mutant animals (Davis et al., 1995; Nelson et al., 2008). Animals heterozygous for the *Hoxa11eGFP* allele were generated by traditional breeding strategies as previously described. LepR-Cre (DeFalco et al., 2001) mice were crossed to the Rosa26-CAG-loxp-stop-loxp-tdTomato (Madisen et al., 2010) line to obtain LepRiTom. To assess spatial variation in bone fracture repair based on local *Hox* expression levels, three distinct fracture-healing models were employed. All animals were anesthetized with isofluorane during each procedure and provided buprenorphine pre- and post-operatively. Carprofen was also given during the recovery period. Post-operative radiographs were taken immediately following fracture (Faxitron X-Ray) to ensure proper fracture location. All animals were fully weight bearing within 1 hour following surgery and were given chow and water ad libitum until the time of death. All animal experiments described in this article were reviewed and approved by the University of Michigan's Committee on Use and Care of Animals, Protocol #08787 (Wellik) and Protocol #09757 (Goldstein).

Fracture Methods

Tibial fracture—Following procedures previously described in detail,(Hiltunen et al., 1993; Taylor et al., 2009) mice were anesthetized with Isofluorane gas, and a small incision was made medial to the tibial tuberosity. A 26-gauge needle was used to bore a small hole into the medial-proximal cortex. The needle was withdrawn and replaced with a sterile 0.009 mm diameter stainless steel wire (McMaster-Carr) that was passed through the marrow space and compacted firmly into the distal tibial bone. The wire was trimmed flush with the cortex, and skin was closed with skin glue. While still anesthetized, mice were placed on a custom guillotine device, with the tibial midshaft placed on top of a two-point support surface. An anvil striker was placed on the anter-medial surface of the tibia at approximately mid-shaft. A weight of ~290 g was dropped from 8 cm to fracture the bone. Tibial "splints" were placed with surgical tape to prevent initial rotational stability of the fracture site over the first 48 hours.

Femoral fracture—Following procedures similar to the tibial fracture, and outlined in rats by Bonnarens and Einhorn (Bonnarens and Einhorn, 1984), a small lateral parapatellar incision was made and the patella was dislocated medially exposing the distal femoral notch. A 26-gauge needle was used to bore a hole into the distal femoral notch. The needle was replaced with a sterile 0.014mm diameter stainless steel wire (McMaster-Carr), which was passed retrograde up through the femoral diaphysis and compacted firmly into the proximal femoral bone. The wire was trimmed flush with the femoral notch, the patella reduced and a suture was used to close the incision through the capsule followed by skin closure using glue. While still anesthetized, mice were placed on a custom guillotine device, with the

femoral midshaft placed on top of a two-point support surface. An anvil striker was placed on the anterior surface of the femur, and a ~290 g weight was dropped from 8 cm to fracture the bone.

Ulnar fracture—A small incision was made along the posterior surface of the ulna. The mid-ulnar diaphysis was exposed via blunt dissection through the overlying soft tissues and periosteum. Using a fine wire cutter, the ulna was cut at the mid-shaft, taking care not to extend the wire cutters into the radius during the fracture process. Skin was closed with skin glue.

X-ray and microCT

X-ray scans were collected using a benchtop x-ray imager by Faxitron at 3X magnification. For timecourse analyses, animals were anesthetized before x-ray imaging. Samples were scanned using an eXplore Locus SP microCT system (GE Healthcare). All specimens were scanned in water using the following parameters: voltage 80 kVp; current 80 μA; exposure time 1600 ms; voxel size in the reconstructed image 18 μm, isotropic. The data were processed and analyzed using MicroView (v2.1.2 Advanced Bone Application; GE Healthcare Preclinical Imaging).

Rating of callus bridging

MicroCT scans were reoriented for analysis and snapshots of the callus were captured in two planes; a transverse plane to capture the radius and ulna together and an orthogonal plane to capture the callus at a 90 degree angle to the transverse plane. Both images were placed side-by-side and blindly rated based on a scale, from 0 to 5, to assess the progression of fracture gap bridging. The following guidelines were used for each score: 0 = bony callus present, not bridged; 1 = woven bone connected on one side of the callus, no cortical bone bridging; 2 = woven bone connected throughout the callus, no cortical bone bridging; 3 = some cortical bone bridging present, woven bone may still be apparent, non-continuous bone marrow space; 4 = predominantly cortical bone bridging, continuous bone marrow space, noticeable callus still present; 5 = exclusively cortical bone bridging, continuous bone marrow space, little to no callus present. Data is presented as a box-and-whisker plot of time points (3 WPF: control n = 5, Hox11 mutant n = 6; 6 WPF: control n = 4, Hox11 mutant n = 6). Statistical analyses were carried out by an unpaired Student’s t-test; * $p<0.05$.

Histology, immunohistochemistry and histomorphometric measurements

Limbs were collected at the indicated ages or time points following fracture surgery. Intramedullary pins were removed if present. All specimens were dissected in PBS on ice and scanned immediately for microCT (if required for fracture analyses). Specimens for frozen sections were fixed for three days in 4% paraformaldehyde in PBS at 4°C, decalcified in 14% EDTA for 7 days and then sunk in 30% Sucrose in PBS overnight prior to embedding into OCT media. Cryosections were collected at 18μm through indicated segments of the limb or through the entire fracture callus.

Immunohistochemical staining was performed using standard methods. Sections were blocked with donkey serum and incubated with primary antibodies overnight at 4°C against

Sox9 (Millipore, AB5535, 1:500), CD44 (Southern Biotech, 1500-01,1:200), PECAM/CD31 (Developmental Studies Hybridoma Bank, 1:10), Perillipin (Sigma, P1873, 1:100), or βIII-tubulin/Tuj-1 (Santa Cruz, sc-58888, 1:100). F4/80 (Abd Serotec, MCA497RT, 1:100) was incubated for 2 hours at 37°C. Secondary antibodies were incubated at room temperature for 2 hours: donkey anti-goat-alexafluor488, donkey-anti-rabbit-alexafluor555, donkey-anti-Armenian hamster-alexafluor594, and donkey-anti-mouse-alexafluor555. To minimize complications resulting from high auto-fluorescence in adult tissues, we used an antibody against GFP (Invitrogen, A-11122, 1:200) followed with either an alkaline phosphatase conjugated (Jackson ImmunoResearch, 111-055-003, 1:500) or an alexafluor488 conjugated (Invitrogen, A21206, 1:1000) anti-rabbit secondary antibody for all above analyses of *Hoxa11eGFP* expression. For *Hoxa11eGFP* co-expression analyses that required rabbit antibodies, tissue was fixed overnight in 4% paraformaldehyde and decalcified for 1–2 days in 14% EDTA before cryoembedding. PDGFRα (Cell Signaling, 3174S, 1:10) or Osterix (Abcam, ab22552, 1:300) primary antibodies were incubated overnight at 4°C in combination with chicken-anti-GFP (Abcam, ab13970, 1:1500). Secondary antibodies were incubated at room temperature for 2 hours: donkey-anti-rabbit-Cy3 and donkey-anti-chicken-488. tdTomato was imaged directly without use of an antibody. TRAP staining was performed using a leukocyte acid phosphatase kit (Sigma).

To quantify the amount of cartilage within each callus, every 10th section from cryopreserved tissue was stained with Safranin O/Fast Green/Hematoxylin as previously described (Kahveci et al., 2000: Tran et al., 2000). The callus area and cartilage area on each section was measure manually using ImageJ software. A minimum of three tissue sections per callus was measured and the average was calculated among all animals per time point (1.5 WPF: control n = 8, *Hox11 mutant* n = 11, 3 WPF: control n = 6, *Hox11 mutant* n = 6; 6 WPF: control n = 7; *Hox11 mutant* n = 6).

All brightfield images were captured on an Olympus BX-51 upright light microscope with an Olympus DP70 camera. Fluorescent images were captured on a Leica Upright SP5X Confocal Microscope with 2-Photon. Confocal Z stacks through entire sections were taken at a thickness of 2μm, stacked using ImageJ software, and stitched together using Photoshop software (when required) to obtain high-resolution images of entire limbs and fracture calluses.

Flow Cytometry

Bone marrow cells were harvested by flushing the marrow cavity with digestion buffer (2mg/mL Collagenase IV and 3mg/mL Dispase in 1xPBS) using an appropriate sized needle for each bone. Periosteum was harvested by careful dissection from the tibia after removing muscle tissue and immediately washing in PBS. To obtain cells from the fracture callus, skin and muscle tissue was carefully dissected away from the callus prior to excision with a razor blade (including cortical bone). The callus/cortical bone tissue was then transferred to a dish with 1ml of digestion buffer and cortical bone was dissected away from the callus. For all dissections, three digestion steps were carried out at 37°C with periodic agitat ion to obtain a single cell suspension. After each period of digestion, cells in suspension were collected into ice-cold staining buffer (1X PBS, 0.5% BSA, 2mM EDTA). Red blood cells were lysed on

ice at a final concentration of 0.5X. For staining, cells were resuspended in staining buffer at a concentration of 1×10^6 cells/30ul in a solution containing the following antibodies: For hematopoietic exclusion; Ter119-AF700 (Biolegend, Clone TER119, 1:100) or TER119-APC (BD, clone TER119, 1:100) and CD45-APCeFluor780 (ebioscience, Clone 30-F11, 1:200) or CD45-APC-Cy7 (BD, clone 30-F11, 1:200). For endothelial cell exclusion: CD31-PerCPCy5.5 (BD, Clone MEC13.3, 1:100) and CD105-PeCy7 (Biolegend, Clone MJ7/18, 1:200). For non-endothelial stroma and MSC exclusion; PDGFRα+/CD140a-APC (ebioscience, Clone APA5, 1:100) or PDGFRα/CD140a-PECF594 (BD, clone APA5, 1:100), CD51-PE (ebioscience, Clone RMV-7, 1:100), Biotinylated-goat-anti-Leptin Receptor (R&D, Cat. BAF497, 1:200), and Streptavidin-Qdot565 (Invitrogen, Cat. Q10133MP, 1:500) or BV605 (Biolegend, 405229, 1:500). For LepR-Cre/tdTomato/*Hoxa11eGFP* samples, cells were collected, digested and stained with CD45-APC-Cy7 and TER119-APC-Cy7 (BD, clone TER119, 1:100) for hematopoietic exclusion. After staining, all samples were washed twice with staining buffer and resuspended in staining buffer with DAPI (1:10,000) for analysis and sorting. Analysis was carried out on an LSRII Fortessa flow cytometer (BD), sorting was performed on a FACSAria II (BD) with 4 lasers (407nm, 488nm, 561nm, 640nm). Results were analyzed with FlowJo (v10.0.7) software.

qRT-PCR for Hox expression

For analysis of expanded, adherent marrow cells, bone marrow was flushed with needles from the tibia, femur, humerus, and radius/ulna of three wild-type animals and cultured separately in DMEM with 4.5 g/L D-glucose (Gibco), 1X Glutamax (Gibco), 1mM Sodium Pyruvate, 15% FBS, 100ug/mL streptomycin, 100U/mL Penicillin. Cells were passaged once and allowed to grow to confluence before they were collected directly into Trizol. RNA was extracted by phenol choloroform. cDNA synthesis was performed with SuperScript II (Invitrogen). For analysis of freshly isolated LepRCre/tdTomato bone marrow cells, bone marrow was digested as described previously and non-hematopoietic, non-endothelial, LepR lineage-positive or negative cells were sorted directly into trizol. RNA was extracted with phenol chloroform and RNeasy micro kit (Qiagen). Due to low cell number collection, cDNA synthesis was performed from the entire sample with EcoDry system (Clontech, random hexamers). *Hox* gene expression was measured relative to Rn18s, and all qPCR was performed with the following primer sets using Roche FastStart SYBR Green Mastermix: Hoxa5F – CAGGGTCTGGTAGCGAGTGT, Hoxa5R – CTCAGCCCCAGATCTACCC; Hoxb6F – GAGACCGAGGAGCAGAAGTG, Hoxb6R – CAGGGTCTGGTAGCGTGTG; Hoxc6F – CCAGGACCAGAAAGCCAGTA, Hoxc6R – CCTTCTCCAGTTCCAGGGTCT; Hoxa9R- GTAAGGGCATCGCTTCTTCC, Hoxa9L – ACAATGCCGAGAATGAGAGC, Hoxb9R – TCCAGCGTCTGGTATTTGGT, Hoxb9L – GAAGCGAGGACAAAGAGAGG, Hoxc9R – AATCTGTCTCTGTCGGCTCC, Hoxc9L – AGTCTGGGCTCCAAAGTCAC, Hoxd9R – TTGTTTGGGTCAAGTTGCTG, Hoxd9: - CTCAGCTTGCAGCGATCA, Hoxa10R – GTGTAAGGGCAGCGTTTCTT, Hoxa10L – CAGCCCCTTCAGAAAACAGT, Hoxc10R – ACCTCTTCTTCCTTCCGCTC, Hoxc10L ACTCCAGTCCAGACACCTCG, Hoxd10R – TTTCCTTCTCCTGCACTTCG, Hoxd10L – GGAGCCCACTAAAGTCTCCC, Hoxa11R – CCTTTTCCAAGTCGCAATGT, Hoxa11L – AGGCTCCAGCCTACTGGAAT, Hoxc11F – GCGGCCGACGAGCTTAT, Hoxc11R –

TTTTTCATGAGGATCTCAGTGACTGT, Hoxd11R – AGTGAGGTTGAGCATCCGAG, Hoxd11L – ACACCAAGTACCAGATCCGC.

Delta Ct values were calculated for each primer set relative to GAPDH or to Rn18s. To analyze each paralogous group (*Hox9*, *Hox10* and *Hox11*) as a whole in cells cultured from stylopod or zeugopod regions, the ratio of stylopod:zeugopod or zeugopod:stylopod was calculated for each primer set in each animal, separately, before it was averaged and graphed.

CFU-F Assays

CFU-F assays were performed either from freshly isolated or from briefly cultured cells. For freshly isolated assays, cells from bone marrow were obtained using a modified version of the method detailed above. Between digestion steps, cells were collected into warm MSC complete media (DMEM with 4.5 g/L D-glucose (Gibco), 1X Glutamax (Gibco), 1mM Sodium Pyruvate, 15% FBS, 100ug/mL streptomycin, 100U/mL Penicillin) supplemented with 2mM EDTA. After all digestions, cells were allowed to rest at 37°C for 10min and cooled on ice before continuing with the above mentioned RBC lysis and staining protocol. 1×10^3-3×10^3 cells were sorted and plated into a single well of a 6-well plate. Cells were maintained at 37°C with 5% CO_2 in a water-jacketed incubator and left untouched for 5 days in phenol red-free D-MEM (Gibco) containing 20% FBS (HyClone), 10% MesenCult stimulatory supplement (STEMCELL Technologies), and 100ug/mL Streptomycin, 100U/mL Penicillin. One-half media was replaced every three days following initial incubation. After 10–14 days, cells were stained with Giemsa and adherent colonies were counted.

For cultured assays, bone marrow from control (*11Aa^{G}DD*) or from Hox11 compound mutant (*11Aa^{G}dd*) animals was flushed and cultured in DMEM (Gibco) containing 1X Glutamax (Gibco), 1mM Sodium Pyruvate (Gibco), 20% FBS (HyClone), 10% Mesencult stimulatory supplement (STEMCELL Technologies), and 100ug/mL Streptomycin, 100U/mL Penicillin for 7 days. 1.5×10^3 non-hematopoietic *Hoxa11eGFP+* cells were sorted and plated in a single well of a 6-well plate. One-half media was replaced every three days following initial incubation. After 10–14 days, cells were stained with Giemsa and adherent colonies were counted.

Tri-lineage differentiation and quantification

To isolate adult *Hoxa11eGFP+* cells, bone marrow from the radius and ulna of adult mice was flushed and bones were minced. In order to test the function of Hox11 from full mutants, cells from whole bones were isolated from E18.5 control and mutant embryos (control: *Hoxa11eGFP+/−*, Mutant: *11aa^{eGFP}dd*). For both isolations, cells were cultured for 7–10 days before sorting for live CD45- (CD45-APC-Cy7) GFP+ cells to plate for differentiation. For chondrogenic differentiation, 5×10^4 cells were plated in micromass, cultured for 21 days (StemPro Chondrogenic differentiation kit) and stained for alcian blue. For osteogenic differentiation,1×10^4 cells were plated in micromass, cultured for 12–14 days (StemPro Osteogenic differentiation kit) and stained for alizarin red. For adipogenic differentiation, 3×10^4 cells/well were plated in monolayer, cultured for 10 days (StemPro

Adipogenic differentiation kit) and stained for oil red O. All experiments were carried out with technical replicates (Adult: 4 Hoxa11eGFP+/− animals; E18.5: 1 control and 1 Hox11 mutant animal). For quantification, captured images were converted to binary format in ImageJ software. For alizarin red and alcian blue stains, the mean intensity of the stain was measured by drawing a box surrounding the colored stain. For oil red O staining, the entire image was measured. Measured mean intensities were normalized to background. Background was calculated by taking an average measurement among three different areas within the image (excluding the stain).

Transplantation Studies

Bone marrow cells from LepRCre/tdTomato/*Hoxa11eGFP* adult animals were expanded in culture with DMEM media containing supplements described above. CD45-/*Hoxa11eGFP*+/tdTomato+ were sorted and recovered in culture for 24 hours prior to transplantation. Tibia fractures were performed on wildtype animals as described above. 3.5×10^5 GFP+/tdTomato + cells were injected 4 days post-fracture in 20μl of 1x sterile PBS. Immunofluorescence for Osterix and Sox9 was performed as described above at 10 days post-fracture.

Supplementary Material

Refer to Web version on PubMed Central for supplementary material.

Acknowledgments

We thank Kathy Sweet and Bonnie Nolan for superb technical assistance during fracture surgeries and post-operative care, John Baker for assistance with plastic processing and histologic staining, and Basma Kouhry and Joseph Petroski for assistance with scanning of microCT specimens. We also thank the University of Michigan core facilities: Flow Cytometry and Microscopy and Image Analysis. We thank Drs. Benjamin Allen, Scott Barolo, Renny Franceschi, Karl Jepsen, Laurie McCauley and numerous Wellik lab members for their advice and critical reading of the manuscript.

We have no disclosures, MTAs, patents or patent applications to report. This work was supported by the following funding sources: National Institutes of Health R01 AR061402 (D.M.W.), T32 DE007057 (D.R.R., K.M.P and J.Y.S.), T32 HD007505 (D.R.R. and K.M.P.), the University of Michigan Summer Biomedical and Life Sciences Fellowship (A.J.S.), the University of Michigan Cell and Developmental Biology Bradley M. Patten Fellowship (D.R.R and K.M.P) and EDGE award from the University of Michigan Endowment for the Basic Sciences (D.R.R.).

REFERENCES

Ackema KB, Charite J. Mesenchymal stem cells from different organs are characterized by distinct topographic Hox codes. Stem cells and development. 2008; 17:979–991. [PubMed: 18533811]

Bianco P, Cao X, Frenette PS, Mao JJ, Robey PG, Simmons PJ, Wang CY. The meaning, the sense and the significance: translating the science of mesenchymal stem cells into medicine. Nature medicine. 2013; 19:35–42.

Bonnarens F, Einhorn TA. Production of a standard closed fracture in laboratory animal bone. J Orthop Res. 1984; 2:97–101. [PubMed: 6491805]

Chang HY, Chi JT, Dudoit S, Bondre C, van de Rijn M, Botstein D, Brown PO. Diversity, topographic differentiation, and positional memory in human fibroblasts. Proceedings of the National Academy of Sciences of the United States of America. 2002; 99:12877–12882. [PubMed: 12297622]

Davis AP, Witte DP, Hsieh-Li HM, Potter SS, Capecchi MR. Absence of radius and ulna in mice lacking hoxa-11 and hoxd-11. Nature. 1995; 375:791–795. [PubMed: 7596412]

DeFalco J, Tomishima M, Liu H, Zhao C, Cai X, Marth JD, Enquist L, Friedman JM. Virus-assisted mapping of neural inputs to a feeding center in the hypothalamus. Science. 2001; 291:2608–2613. [PubMed: 11283374]

Frenette PS, Pinho S, Lucas D, Scheiermann C. Mesenchymal stem cell: keystone of the hematopoietic stem cell niche and a stepping-stone for regenerative medicine. Annual review of immunology. 2013; 31:285–316.

Fromental-Ramain C, Warot X, Lakkaraju S, Favier B, Haack H, Birling C, Dierich A, Doll e P, Chambon P. Specific and redundant functions of the paralogous Hoxa-9 and Hoxd-9 genes in forelimb and axial skeleton patterning. Development. 1996a; 122:461–472. [PubMed: 8625797]

Fromental-Ramain C, Warot X, Messadecq N, LeMeur M, Dolle P, Chambon P. Hoxa-13 and Hoxd-13 play a crucial role in the patterning of the limb autopod. Development. 1996b; 122:2997–3011. [PubMed: 8898214]

Gerstenfeld LC, Cullinane DM, Barnes GL, Graves DT, Einhorn TA. Fracture healing as a post-natal developmental process: molecular, spatial, and temporal aspects of its regulation. J Cell Biochem. 2003; 88:873–884. [PubMed: 12616527]

Hiltunen A, Vuorio E, Aro HT. A standardized experimental fracture in the mouse tibia. J Orthop Res. 1993; 11:305–312. [PubMed: 8483044]

Kahveci Z, Minbay FZ, Cavusoglu L. Safranin O staining using a microwave oven. Biotechnic & histochemistry : official publication of the Biological Stain Commission. 2000; 75:264–268. [PubMed: 11131567]

Kfoury Y, Scadden DT. Mesenchymal cell contributions to the stem cell niche. Cell Stem Cell. 2015; 16:239–253. [PubMed: 25748931]

Kunisaki Y, Bruns I, Scheiermann C, Ahmed J, Pinho S, Zhang D, Mizoguchi T, Wei Q, Lucas D, Ito K, et al. Arteriolar niches maintain haematopoietic stem cell quiescence. Nature. 2013; 502:637–643. [PubMed: 24107994]

Leucht P, Kim JB, Amasha R, James AW, Girod S, Helms JA. Embryonic origin and Hox status determine progenitor cell fate during adult bone regeneration. Development. 2008; 135:2845–2854. [PubMed: 18653558]

Lonfat N, Duboule D. Structure, function and evolution of topologically associating domains (TADs) at HOX loci. FEBS letters. 2015; 589:2869–2876. [PubMed: 25913784]

Madisen L, Zwingman TA, Sunkin SM, Oh SW, Zariwala HA, Gu H, Ng LL, Palmiter RD, Hawrylycz MJ, Jones AR, et al. A robust and high-throughput Cre reporting and characterization system for the whole mouse brain. Nature neuroscience. 2010; 13:133–140. [PubMed: 20023653]

Mallo M, Wellik DM, Deschamps J. Hox genes and regional patterning of the vertebrate body plan. Dev Biol. 2010; 344:7–15. [PubMed: 20435029]

Mizoguchi T, Pinho S, Ahmed J, Kunisaki Y, Hanoun M, Mendelson A, Ono N, Kronenberg HM, Frenette PS. Osterix marks distinct waves of primitive and definitive stromal progenitors during bone marrow development. Dev Cell. 2014; 29:340–349. [PubMed: 24823377]

Montavon T, Duboule D. Chromatin organization and global regulation of Hox gene clusters. Philosophical transactions of the Royal Society of London Series B, Biological sciences. 2013; 368:20120367. [PubMed: 23650639]

Nelson LT, Rakshit S, Sun H, Wellik DM. Generation and expression of a Hoxa11eGFP targeted allele in mice. Dev Dyn. 2008; 237:3410–3416. [PubMed: 18942146]

Park D, Spencer JA, Koh BI, Kobayashi T, Fujisaki J, Clemens TL, Lin CP, Kronenberg HM, Scadden DT. Endogenous bone marrow MSCs are dynamic, fate-restricted participants in bone maintenance and regeneration. Cell Stem Cell. 2012; 10:259–272. [PubMed: 22385654]

Pineault KM, Swinehart IT, Garthus KN, Ho E, Yao Q, Schipani E, Kozloff KM, Wellik DM. Hox11 genes regulate postnatal longitudinal bone growth and growth plate proliferation. Biology open. 2015; 4:1538–1548. [PubMed: 26500224]

Pinho S, Lacombe J, Hanoun M, Mizoguchi T, Bruns I, Kunisaki Y, Frenette PS. PDGFRalpha and CD51 mark human nestin+ sphere-forming mesenchymal stem cells capable of hematopoietic progenitor cell expansion. J Exp Med. 2013; 210:1351–1367. [PubMed: 23776077]

Raines AM, Magella B, Adam M, Potter SS. Key pathways regulated by HoxA9,10,11/HoxD9,10,11 during limb development. BMC Dev Biol. 2015; 15:28. [PubMed: 26186931]

Rinn JL, Bondre C, Gladstone HB, Brown PO, Chang HY. Anatomic demarcation by positional variation in fibroblast gene expression programs. PLoS genetics. 2006; 2:e119. [PubMed: 16895450]

Rinn JL, Wang JK, Allen N, Brugmann SA, Mikels AJ, Liu H, Ridky TW, Stadler HS, Nusse R, Helms JA, et al. A dermal HOX transcriptional program regulates site-specific epidermal fate. Genes Dev. 2008; 22:303–307. [PubMed: 18245445]

Schindeler A, McDonald MM, Bokko P, Little DG. Bone remodeling during fracture repair: The cellular picture. Semin Cell Dev Biol. 2008; 19:459–466. [PubMed: 18692584]

Shapiro F. Bone development and its relation to fracture repair. The role of mesenchymal osteoblasts and surface osteoblasts. European cells & materials. 2008; 15:53–76. [PubMed: 18382990]

Swinehart IT, Schlientz AJ, Quintanilla CA, Mortlock DP, Wellik DM. Hox11 genes are required for regional patterning and integration of muscle, tendon and bone. Development. 2013; 140:4574–4582. [PubMed: 24154528]

Taylor DK, Meganck JA, Terkhorn S, Rajani R, Naik A, O'Keefe RJ, Goldstein SA, Hankenson KD. Thrombospondin-2 influences the proportion of cartilage and bone during fracture healing. J Bone Miner Res. 2009; 24:1043–1054. [PubMed: 19123916]

Tran D, Golick M, Rabinovitz H, Rivlin D, Elgart G, Nordlow B. Hematoxylin and safranin O staining of frozen sections. Dermatologic surgery : official publication for American Society for Dermatologic Surgery [et al]. 2000; 26:197–199.

Wellik DM, Capecchi MR. Hox10 and Hox11 genes are required to globally pattern the mammalian skeleton. Science. 2003; 301:363–367. [PubMed: 12869760]

Worthley DL, Churchill M, Compton JT, Tailor Y, Rao M, Si Y, Levin D, Schwartz MG, Uygur A, Hayakawa Y, et al. Gremlin 1 identifies a skeletal stem cell with bone, cartilage, and reticular stromal potential. Cell. 2015; 160:269–284. [PubMed: 25594183]

Zhou BO, Yue R, Murphy MM, Peyer JG, Morrison SJ. Leptin-receptor-expressing mesenchymal stromal cells represent the main source of bone formed by adult bone marrow. Cell Stem Cell. 2014; 15:154–168. [PubMed: 24953181]

Highlights

- Regional adult skeletal *Hox* expression mirrors that established during development.
- *Hox* gene expression in the adult skeleton is exclusively in progenitor-enriched MSCs.
- Loss of *Hox11* gene function impairs differentiation to chondrocytes and osteoblasts.
- *Hox11* mutant mice show region-specific defects in fracture repair of the skeleton.

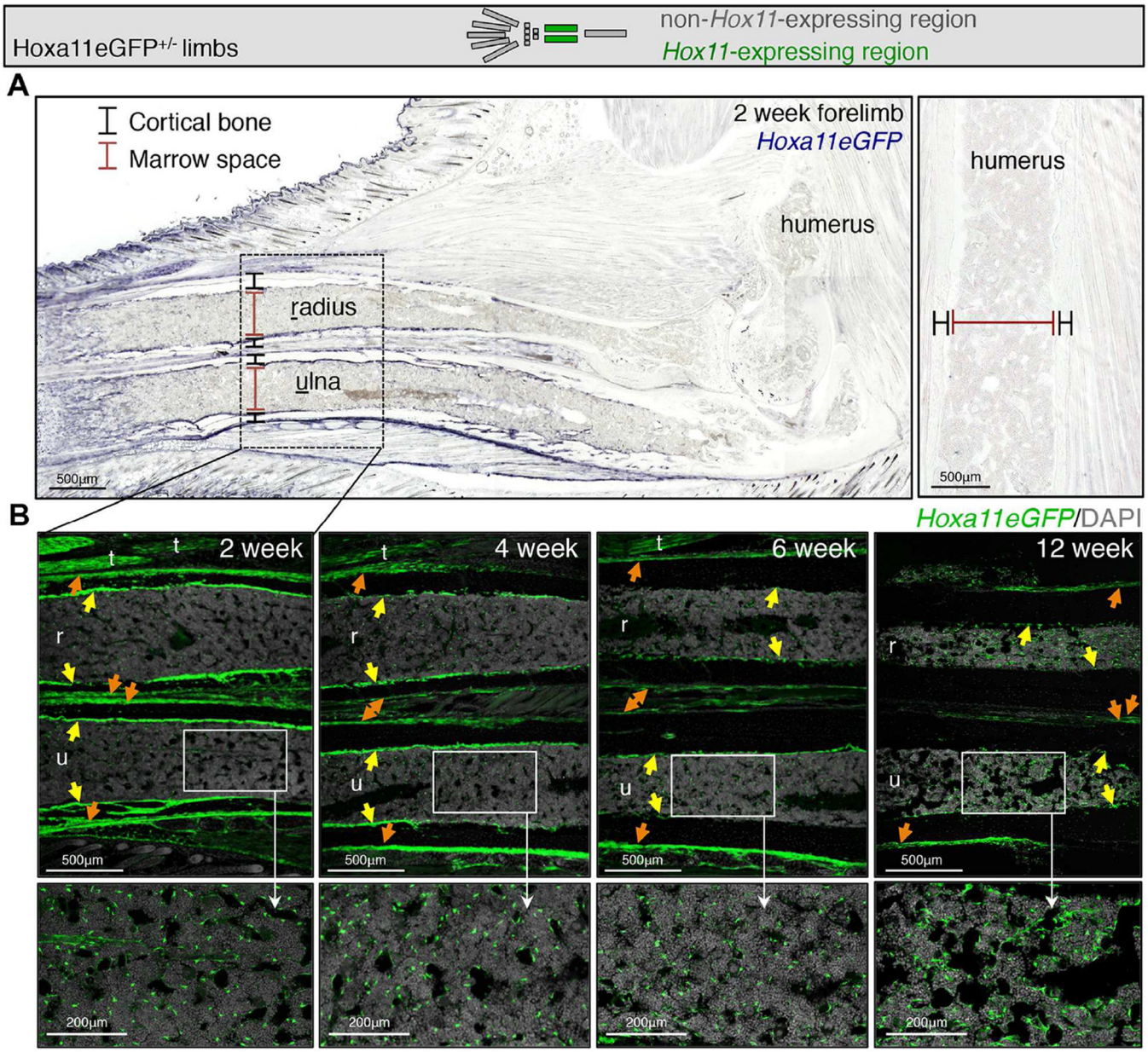

Figure 1. *Hox11* expression is maintained regionally through postnatal and adult stages

Limb schematic depicts Hoxa11eGFP regional expression (green).

(A) Low magnification images of the forelimb at 2 weeks show that Hoxa11eGFP expression is restricted to the zeugopod and absent from the stylopod. See also Figure S2.

(B) High magnification images show strong periosteal expression (orange arrows) through postnatal stages and into adulthood. Hoxa11eGFP expression is additionally observed in endosteal regions (yellow arrows) and in the bone marrow (higher magnification insets). (r) radius; (u) ulna; (t) tendon. See also Figure S2.

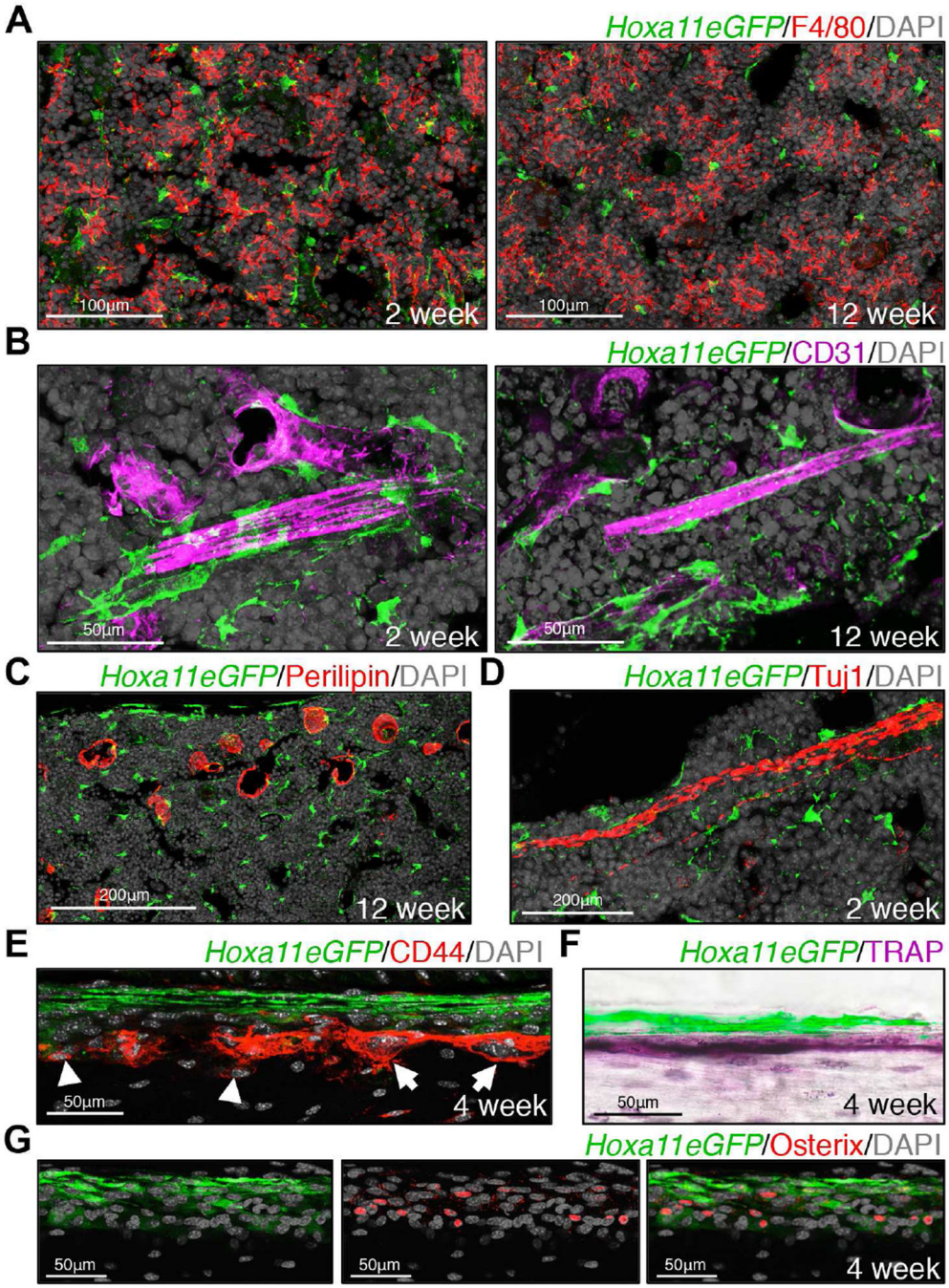

Figure 2. *Hox11* is not expressed in differentiated cell types

Co-expression analyses using known markers for differentiated cell types and Hoxa11eGFP.

(A) Hoxa11eGFP is excluded from F4/80+ macrophages in bone marrow.

(B) Hoxa11eGFP is excluded from CD31+ endothelial cells, but GFP+ cells closely associate with bone marrow vasculature.

(C) Hoxa11eGFP is excluded from Perillipin+ adipocytes in bone marrow.

(D) Hoxa11eGFP is excluded from Tuj1+ neurons in the bone marrow.

(E–G) Hoxa11eGFP is excluded from CD44+ small, mononucleate osteoblasts (arrow heads) and from CD44+ large, multinucleate osteoclasts (arrows) on the bone surface (E). Co-expression analysis of Hoxa11eGFP using TRAP (osteoclasts, F) and Osterix (osteoblasts, G) are consistent with CD44 staining.

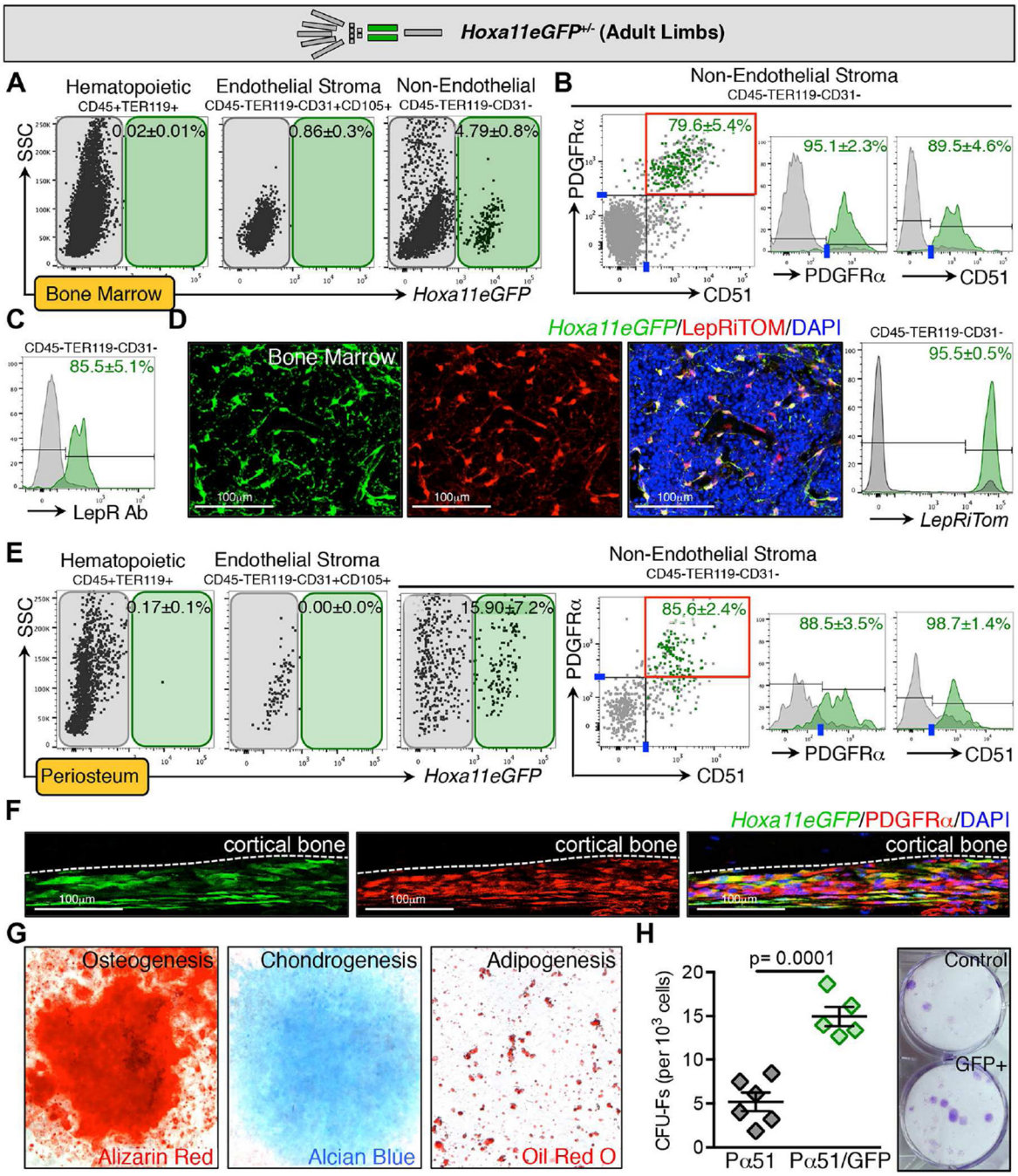

Figure 3. Hoxa11eGFP-expressing cells are a subset of bone marrow mesenchymal stem/stromal cells (BM-MSCs)

Limb schematic depicts Hoxa11eGFP regional expression (green).

(A–B) FACS analysis of live bone marrow cells from unfractured zeugopod skeleton reveals *Hoxa11eGFP* is not expressed in CD45+/TER119+ hematopoietic cells or in CD105+/CD31+ endothelial cells. Hoxa11eGFP is expressed in CD45-/TER119-/CD31-non-endothelial stromal cells. Overlaid FACS plots or histograms display GFP+ (green) and GFP- (gray) cells from non-endothelial stromal compartment. Hoxa11eGFP-positive cells

predominantly sort with the PDGFRα+ and CD51+ cells. Data are represented as mean ± SEM. See also Figures S3A and B and Figure S4B.

(C) Using an antibody against Leptin Recteptor (LepR), FACS analysis shows that Hoxa11eGFP-positive cells are also marked by LepR. Data are represented as mean ± SEM.

(D) Mice carrying alleles for *Hoxa11eGFP*, *LepR-Cre*, and *ROSA-tdTomato* show high overlap of Hoxa11eGFP-positive and LepRiTom+ cells in immunofluorescent sections. Analogous FACS analysis shows that 95.5±0.5% of all GFP+ cells are also LepRiTom+. Data are represented as mean ± SEM. See also Figure S4A.

(E) FACS analysis of live periosteal cells shows that Hoxa11eGFP-positive cells are also non-hematopoietic, non-endothelial cells that co-express PDGFRα and CD51. See also Figure S3C.

(F) Immunofluoresence for PDGFRα shows co-expression of Hoxa11eGFP+ cells and PDGFRα in the periosteum.

(G) *In vitro* analyses reveal that sorted Hoxa11eGFP+ bone marrow cells are capable of tri-lineage differentiation.

(H) Sorted Hoxa11eGFP+/PDGFRα+/CD51+ cells exhibit increased CFU-F formation compared to cells sorted only as PDGFRα+/CD51+. Data are represented as mean ± SEM.

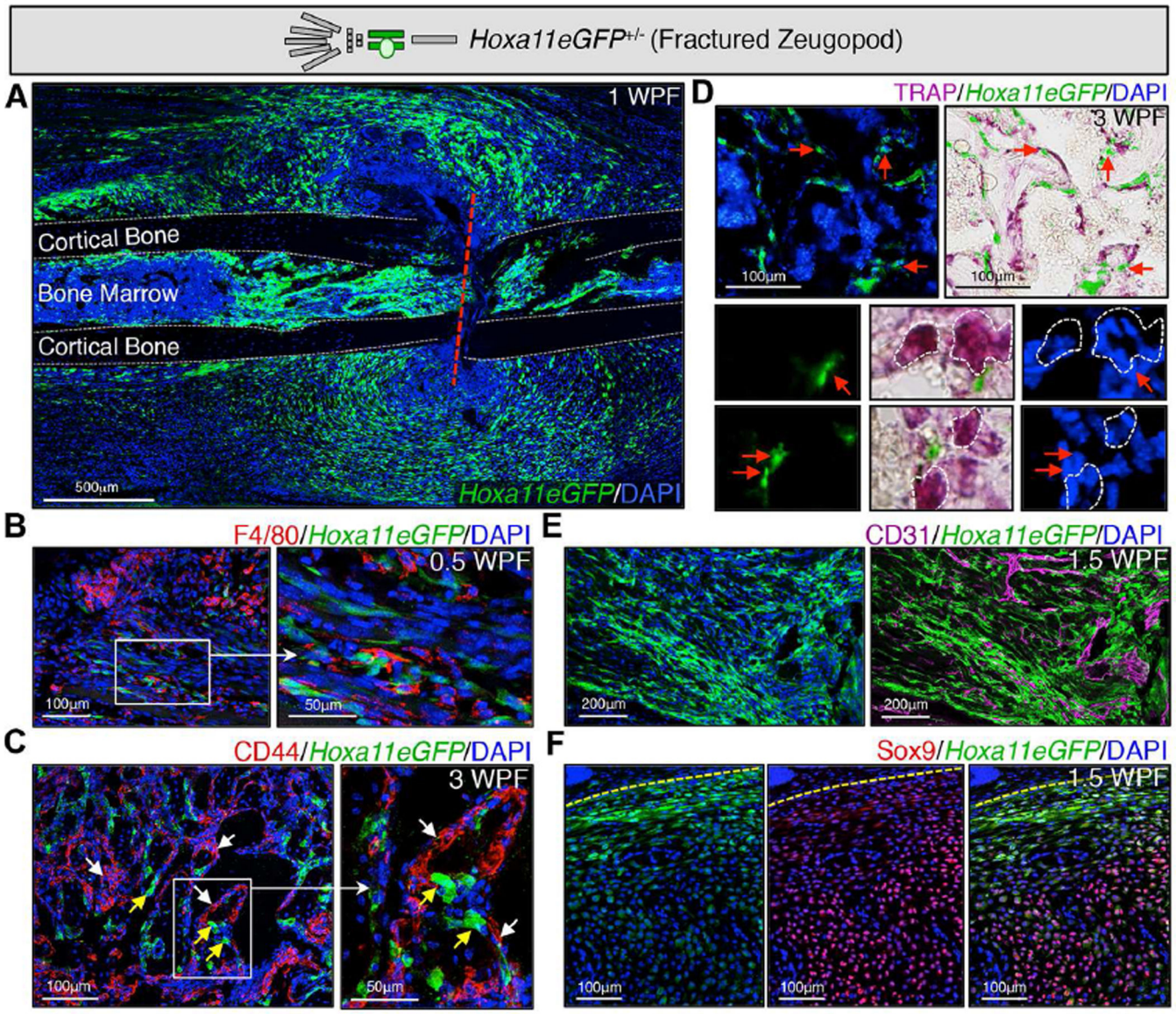

Figure 4. *Hoxa11eGFP*-expressing cells expand following injury and do not overlap with differentiated cell types

Limb schematic depicts Hoxa11eGFP regional expression (green) and the fracture callus in the zeugopod region (ulna or tibia). Fractures were performed in the zeugopod region (ulna or tibia) of *Hoxa11eGFP* heterozygous mice.

(A) At 1 week post-fracture (WPF), Hoxa11eGFP+ cells can be visualized at the site of fracture (red dashed line) expanded in the forming callus. (dashed grey line) outline of cortical bone.

(B) At 0.5WPF, Hoxa11eGFP does not overlap with F4/80+ macrophages.

(C) At 3WPF, Hoxa11eGFP-expressing cells are near bone surfaces and excluded from CD44+ osteoblasts and osteoclasts.

(D) At 3WPF, Hoxa11eGFP-expressing cells are distinct from TRAP+ osteoclasts, but are closely associated with them near the bone surface.

(E) At 1.5WPF, Hoxa11eGFP is excluded from CD31+ endothelial cells, but are closely associated with new vasculature in the callus.
(F) At 1.5WPF, Hoxa11eGFP is highly expressed in the expanded periosteum (yellow dashed line) surrounding the callus and dramatically decreases as Sox9 expression increases in differentiating chondrocytes closer to the center of the callus.

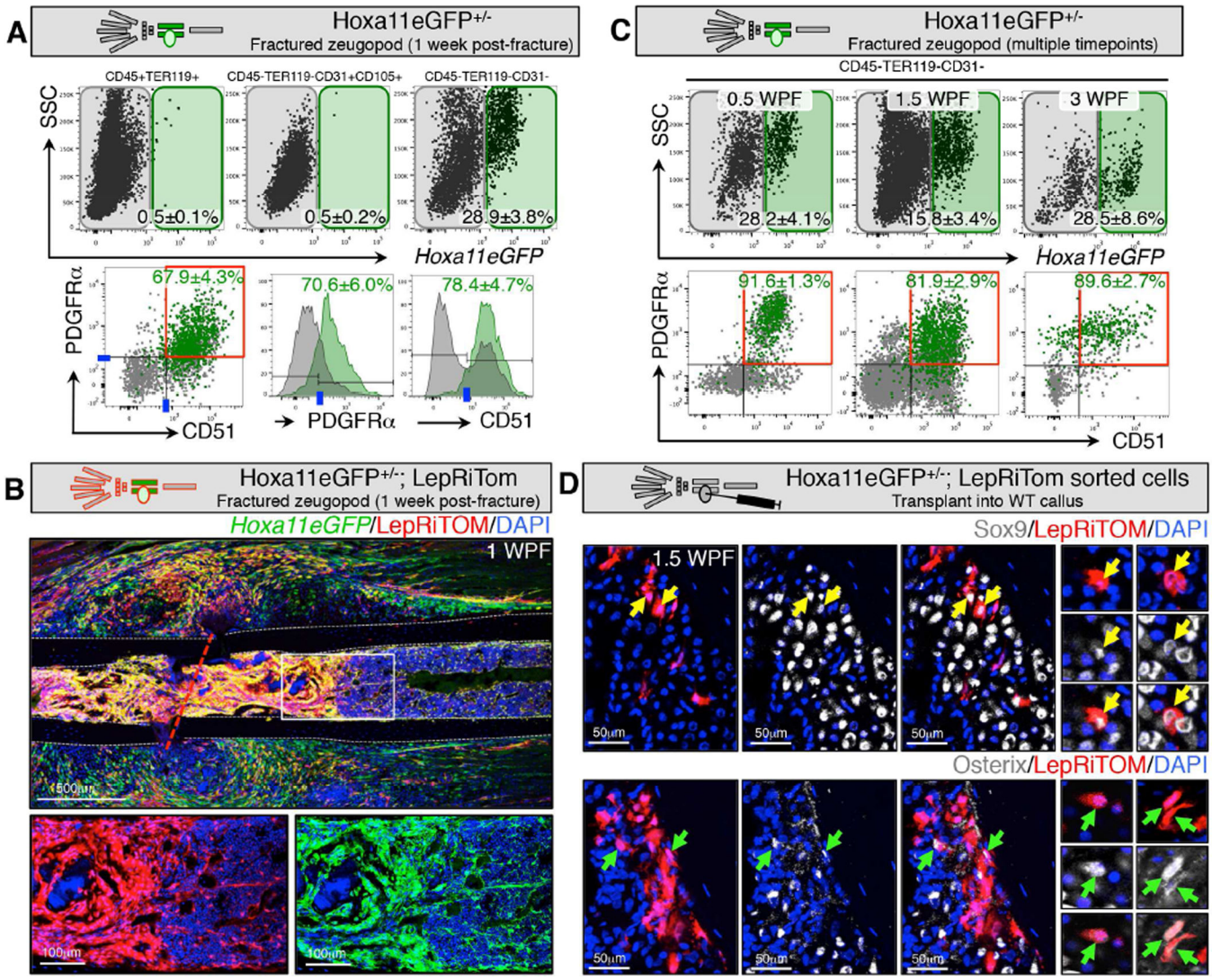

Figure 5. Hoxa11eGFP-expressing cells in the fracture callus are progenitors that give rise to differentiated cell types

Limb schematic depicts Hoxa11eGFP regional expression (green) and the fracture callus in the zeugopod region (tibia or ulna). Fractures were performed in the zeugopod region (ulna or tibia) of *Hoxa11eGFP*+/− mice.

(A) Live-cell FACS analysis of the callus at 1WPF, reveals that Hoxa11eGFP is not expressed in CD45+/TER119+ hematopoietic cells or in CD105+/CD31+ endothelial cells. Hoxa11eGFP is expressed in CD45-/TER119-/CD31- non-endothelial stromal cells. Overlaid FACS plots and histograms display GFP+ (green) and GFP- (gray) cells from the non-endothelial stromal compartment. Hoxa11eGFP+ cells are predominantly in the PDGFRα+/CD51+ progenitor population. Data are represented as mean ± SEM.

(B) Mice carrying alleles for *Hoxa11eGFP*, *LepRCre*, and *ROSA-tdTomato* show overlap of Hoxa11eGFP+ and LepRiTom+ cells in immunofluorescence sections during fracture healing, especially in the expanded bone marrow population closest to the fracture site (higher magnification images). (dashed grey line) outline of cortical bone, (red dashed line) fracture line.

(C) Live-cell FACS analysis at 0.5WPF, 1.5WPF, and at 3WPF reveals that Hoxa11eGFP is expressed in PDGFRα+/CD51+ cells at all stages of repair. Data are represented as mean ± SEM. See also Figure S5A and B.

(D) Sorted, bone marrow LepRiTom+(*LepR-Cre* lineage trace)/Hoxa11eGFP+ cells transplanted into a wildtype, 4-day old tibia fracture callus are capable of differentiating to Sox9+ chondrocytes (top, yellow arrows) and Osterix (Osx)+ osteoblasts (bottom, green arrows) at 10 days post-fracture (6 days post-injection). Higher magnification images show single tdTomato+ cells from additional sections that co-express either Sox9 (top, yellow arrows) or Osx (bottom, green arrows).

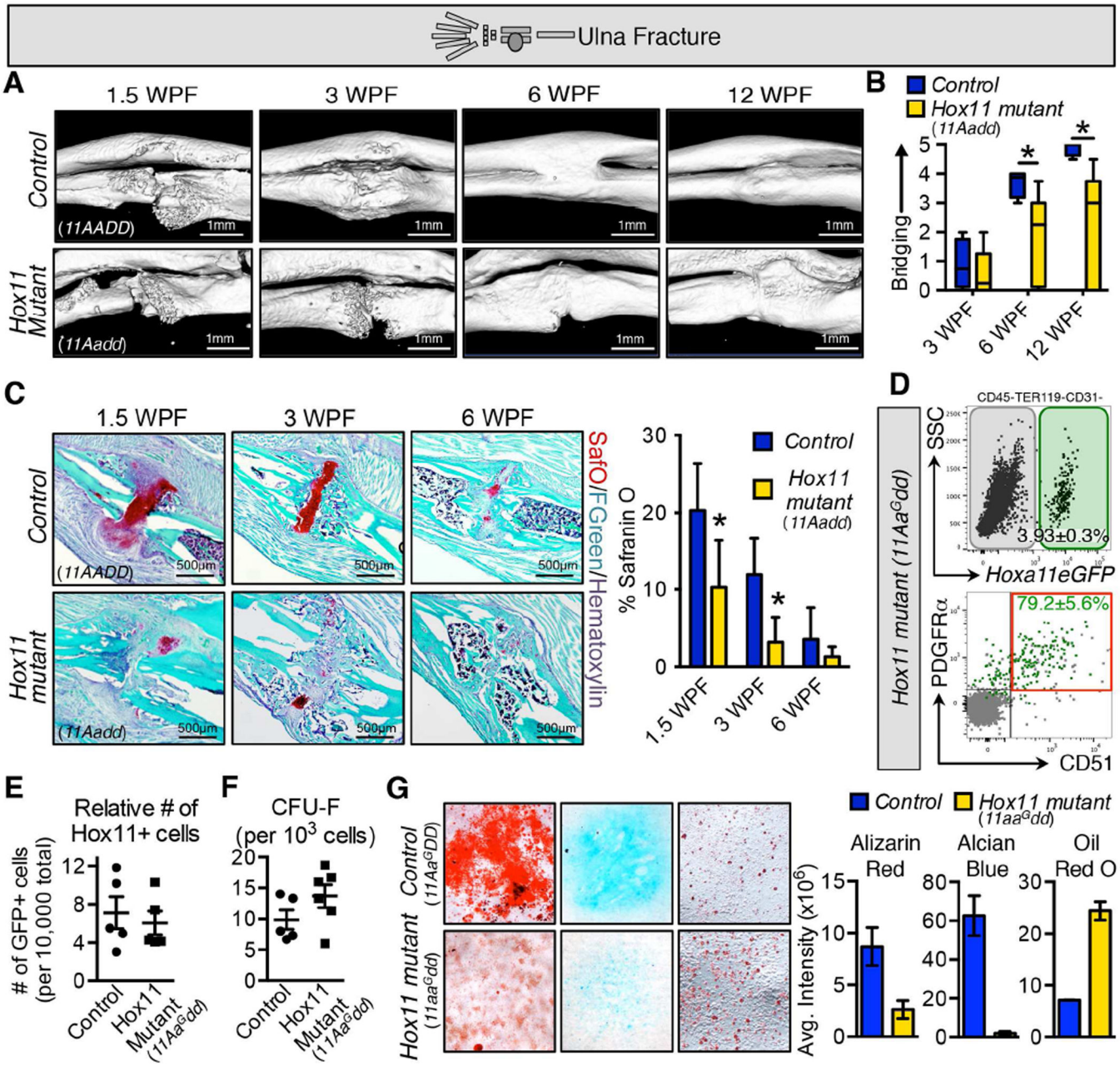

Figure 6. Loss of *Hox11* function impairs fracture healing *in vivo* and results in *in vitro* differentiation defects

Limb schematic depicts placement of the fracture in the ulna of control and *Hox11* compound mutant mice (*11Aadd*).

(A) MicroCT isosurfaces reveal the overall visual defect in repair of *Hox11* mutants (*11Aadd*, lower panels) compared to controls (*11AADD*, upper panels).

(B) Blinded scoring of microCT saggital and coronal images highlight the defects in bridging of the fracture gap in mutants (*11Aadd*, yellow) compared to controls (*11AADD*, blue). Statistics represented with a student T-test; * $p<0.05$.

(C) Safranin O staining and quantification at 3 timepoints post-fracture show a significant decrease in the amount of cartilage formed in the *Hox11* mutant (*11Aadd*) callus. Statistics represented with a student T-test; * $p<0.05$.

(D) Hoxa11eGFP+ cells from the bone marrow of adult *Hox11* compound mutant (*11Aa^{G}dd*) animals are PDGFRα+/CD51+ non-endothelial stromal cells. Data are represented as mean ± SEM. See also Figure S6A and B.

(E) The relative number of Hoxa11eGFP+ cells from the bone marrow or control (*11Aa^{G}DD*) and *Hox11* compound mutant (*11Aa^{G}dd*) animals is unchanged. Data is represented as number of GFP+ cells per 10,000 live cells.

(F) The CFU-F capacity of Hoxa11eGFP+ cells from the bone marrow of control (*11Aa^{G}DD*) and *Hox11* compound mutant (*11Aa^{G}dd*) animals is unchanged. Data is represented as number of colonies per 1,000 GFP+ sorted cells.

(G) *In vitro* tri-lineage differentiation analysis was performed on sorted Hoxa11eGFP+ cells from E18.5 control (*Hox11Aa^{G}DD*) and *Hox11* mutant (*Hox11aa^{G}dd*) animals. Hoxa11eGFP+ cells from *Hox11* mutant animals (yellow) have decreased capacity for osteogenic and chondrogenic differentiation in micromass and increased capacity for adipogenic differentiation compared to controls (blue). Data represented as average staining intensity quantified using ImageJ software. Statistics represented with a student T-test; * $p<0.05$.

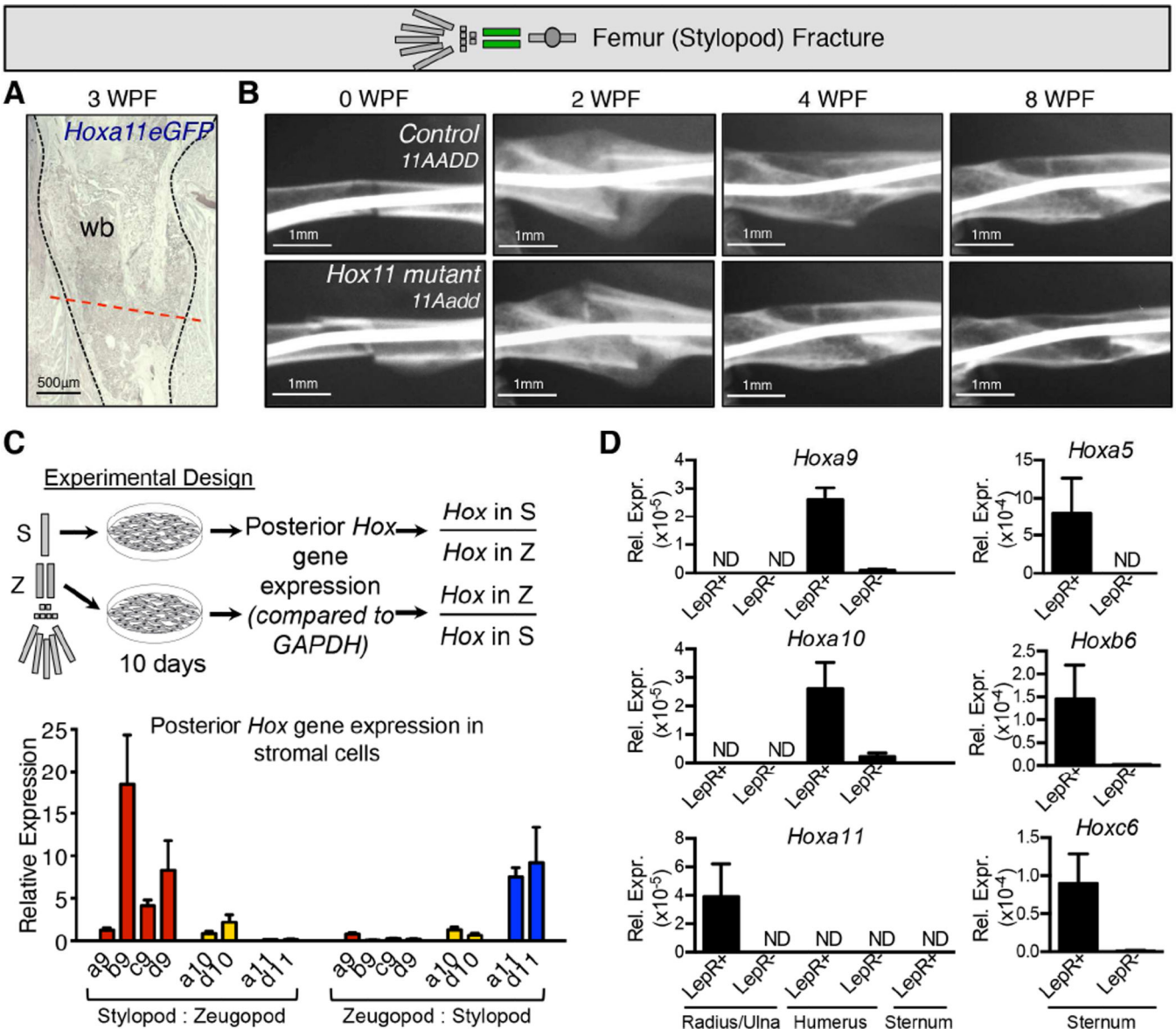

Figure 7. *Hox* expression and function is regionally restricted

(A–B) Limb schematic depicts Hoxa11eGFP regional expression (green) and placement of the fracture in the femur. (A) Femur fractures were performed in *Hoxa11eGFP* heterozygous (control) and *Hox11* compound mutant mice to assess regional specificity of *Hox11* expression and function. No ectopic Hoxa11eGFP expression occurs in response to femur fracture. (wb) woven bone; (dashed black line) outline of fracture. See also Figure S7. (B) A time course of X-ray analyses shows that loss of *Hox11* function does not affect the rate of repair of a femur fracture (*11Aadd*, bottom panels) compared to controls (*11AADD*, top panels).

(C) The posterior *Hox* expression profile (*Hox9-11*) was assessed in cultured bone marrow stromal cells. A schematic of the experiment is shown: bone marrow from adult stylopods and zeugopod was expanded *in* vitro for 10 days to enrich for stroma before performing qRT-PCR. The fold change (relative to GADPH) for each *Hox* gene in each limb segement

(stylopod or zeugopod) was calculated for each animal. Results of the experiment show expression profiles of the posterior *Hox* genes in adult bone marrow stromal cells compliment the expression patterns established during development.
(D) Sorted CD45-TER119-CD31-LepRiTom+ and LepRiTom- cells from the bone marrow of various skeletal elements were analyzed by qPCR for *Hox* expression. *Hoxa9* and *Hoxa10* are exclusively expressed in the LepR+ bone marrow cells from the humerus and not in the radius/ulna. *Hoxa11* is exclusively expressed in LepR+ cells from the radius/ulna and not in the humerus or the sternum. *Hox5* and *Hox6* genes are expressed in the sternum. In all analyses, *Hox* expression is only detected in LepR+ cells. Data is represented relative to housekeeping gene, Rn18s, using the ΔΔcT method.